Lagrangian Coherent Structures in the Elliptic Restricted Three-Body Problem

Evan S. Gawlik
Control and Dynamical Systems
California Institute of Technology 107-81
Pasadena, CA 91125
email: egawlik@caltech.edu

Jerrold E. Marsden
Control and Dynamical Systems
California Institute of Technology 107-81
Pasadena, CA 91125
email: marsden@cds.caltech.edu

Philip C. Du Toit
Control and Dynamical Systems
California Institute of Technology 107-81
Pasadena, CA 91125
email: pdutoit@cds.caltech.edu

Stefano Campagnola
Aerospace and Mechanichal Engineering
University of Southern California
854 Downey Way
Los Angeles, CA 90089-1191
email: scampagn@usc.edu

This version: 7 April 2008

Abstract

This study investigates Lagrangian coherent structures (LCS) in the elliptic restricted three-body problem (ER3BP), a generalization of the circular restricted three-body problem (CR3BP) that asks for the motion of a test particle in the presence of two elliptically orbiting point masses. Previous studies demonstrate that an understanding of transport phenomena in the CR3BP, an autonomous dynamical system (when viewed in a rotating frame), can be obtained through analysis of the stable and unstable manifolds of certain periodic solutions to the CR3BP equations of motion. These invariant manifolds form cylindrical tubes within surfaces of constant energy that act as separatrices between orbits with qualitatively different behaviors. The computation of LCS, a technique typically applied to fluid flows to identify transport barriers in the domains of time-dependent velocity fields, provides a convenient means of determining the time-dependent analogues of these invariant manifolds for the ER3BP, whose equations of motion contain an explicit dependency on the independent variable. As a direct application, this study uncovers the contribution of the planet Mercury to the Interplanetary Transport Network, a network of tubes through the solar system that can be exploited for the construction of low-fuel spacecraft mission trajectories.

Contents

1 Introduction **2**
1.1 The Circular and Elliptical Restricted Three-Body Problems 3
1.2 Invariant Manifolds 6
1.3 Lagrangian Coherent Structures (LCS) 7

2 Computational Methodology **8**
2.1 Poincaré Maps and the Finite-Iteration Lyapunov Exponent 9
2.2 The Finite-Time Lyapunov Exponent 9
2.3 A Comparison Using the Circular Restricted Three-Body Problem (CR3BP) as a Test Bed 10

3 Lagrangian Coherent Structures (LCS) in the Elliptic Restricted Three-Body Problem (ER3BP) **11**
3.1 A Test Case 13
3.2 LCS in the Earth-Moon System 14
3.3 Mercury and the BepiColombo Mission 14

4 Conclusions and Further Study **16**

1 Introduction

The three-body problem is a dynamical system rich in mathematical intricacy and practical applicability. A classic problem in the study of celestial mechanics, the general three-body problem asks for the motion of three masses in space under mutual gravitational interaction. The benefit to investigating the three-body problem is twofold: results of such studies often bear broader implications in the theory of dynamical systems, and the investigations themselves are patently well-suited to address challenges in astronomy. In particular, obtaining a global picture of the dynamical barriers that govern the transport of material through a celestial system is an issue of import to scientists in a surprisingly wide range of fields [1, 2]. The main goal of this paper is to use the theory of Lagrangian coherent structures introduced by Haller [3] to determine transport barriers in the elliptic restricted three-body problem (ER3BP).

Koon and co-authors [4] demonstrate that an understanding of transport phenomena in the circular restricted three-body problem (CR3BP), a problem that asks for the motion of a test particle in the presence of two circularly orbiting point masses, can be obtained through investigation of the stable and unstable manifolds of certain periodic solutions to the three-body problem equations of motion. Evidently, a globalization of the stable and unstable manifolds of periodic orbits about the L_1 and L_2 Lagrange points (unstable equilibrium points in the the CR3BP) reveals a web of tubes through phase space that form separatrices between its dynamically different regions. This labyrinth of tubes, dubbed an "Interplanetary Transport Network" [5], can be exploited in a variety of ways, including the explanation of unusual comet trajectories [6], the investigation of transport of material throughout the solar system [7], and the construction of orbits with prescribed itineraries for low-fuel spacecraft mission trajectories [8].

Elaborating on the latter notion, the complexities of multi-body dynamics recently have begun to play an increasingly more prominent role in the realm of space mission design [5]. Substantial improvements in fuel efficiency for certain classes of missions can be achieved through an exploitation of the natural dynamics of the three-body problem [8]. NASA's Genesis Discovery mission, for instance, exploited subtleties in the dynamics of the Sun-Earth-spacecraft three-body system to traverse a route whose intracacies simpler models like the patched conic approximation fail to describe adequately [9].

Computational methods for determining the invariant manifolds of dynamical systems are well-developed for autonomous systems of differential equations like those describing the CR3BP [10]. When we turn our attention to non-autonomous differential equations, the methods available for computing stable and unstable manifolds are no longer applicable, as the notions of stable and unstable manifolds for time-dependent vector fields are not even well-defined. Such is the case in the elliptic restricted three-body problem, where no choice of reference frame can rid the differential equations of motion of their time dependency. However, Shadden and co-authors [11] shed light on this issue in their development of the theory of Lagrangian coherent structures (LCS) for time-dependent flows. In their report, the authors provide a rigorous justification that LCSs–transport barriers in the domains of time-dependent velocity fields that can be computed algorithmically–"represent nearly invariant manifolds even in systems with arbitrary time dependence" under suitable conditions [11].

This report consists of two parts. Section 2 compares two methods of LCS computation applied to the circular restricted three-body problem. The method deemed superior is used in Section 3 to compute LCS in three different elliptic restricted three-body systems: a system described by fabricated mass and orbital eccentricity parameters, the Earth-Moon-spacecraft system, and the Sun-Mercury-spacecraft system.

1.1 The Circular and Elliptical Restricted Three-Body Problems

This section studies the *restricted three-body problem*, starting with the case when the two primaries are in circular orbit and then the case when the primaries are in elliptical orbits.

The Circular Restricted Three-Body Problem (CR3BP). The circular restricted three-body problem (CR3BP) considers the motion of a test mass $m_3 = 0$ in the presence of the gravitational field of two primary masses $m_1 = 1 - \mu$ and $m_2 = \mu$ in circular orbit about their center of mass. Throughout the paper, the test particle is assumed to begin in the orbital plane of the two primary masses with its velocity component normal to that plane equal to zero, so that its motion is constrained to the m_1-m_2 orbital plane for all time. Without loss of generality, all units are normalized and positions are defined relative to a rotating coordinate frame whose x-axis coincides with the line joining m_1 and m_2 and whose origin coincides with the center of mass of m_1 and m_2, as shown in Fig. 1.1. The equations of motion for the test particle are then [12]

$$\ddot{x} - 2\dot{y} = \frac{\partial \Omega}{\partial x} \tag{1.1}$$

$$\ddot{y} + 2\dot{x} = \frac{\partial \Omega}{\partial y}, \tag{1.2}$$

where

$$\Omega(x, y) = \frac{x^2 + y^2}{2} + \frac{1 - \mu}{\sqrt{(x + \mu)^2 + y^2}} + \frac{\mu}{\sqrt{(x - 1 + \mu)^2 + y^2}} + \frac{1}{2}\mu(1 - \mu) \tag{1.3}$$

and (x, y) denotes the position of m_3 in the rotating frame.

There are five equilibrium points (Lagrange points) L_i, $i = 1, 2, 3, 4, 5$, in the CR3BP [12], corresponding to critical points of the effective potential Ω. Three of these points (L_1, L_2, and L_3) are collinear with the masses m_1 and m_2, while the remaining two (L_4 and L_5) lie at the vertices of

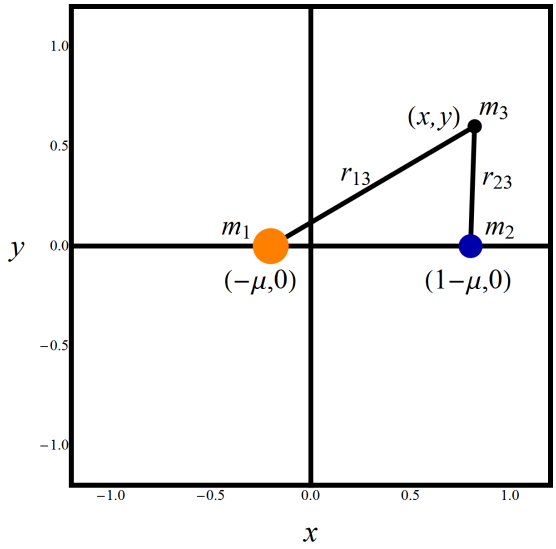

Figure 1.1: Rotating coordinate system in the circular restricted three-body problem. All units are nondimensionalized. The coordinate frame rotates counterclockwise with unit angular frequency. In the case of the elliptic restricted three-body problem, the picture is the same, but the frame rotates nonuniformly and pulsates isotropically in x and y to ensure that the primary masses remain fixed at the positions $(-\mu, 0)$ and $(1-\mu, 0)$.

the pair of equilateral triangles whose bases coincide with the line segment joining m_1 and m_2 (see Fig. 1.2(b)). Let L_i^x and L_i^y denote the x and y coordinates, respectively, of i^{th} Lagrange point.

It is straightforward to check through differentiation that

$$E(x, y, \dot{x}, \dot{y}) = \frac{1}{2}(\dot{x}^2 + \dot{y}^2) - \Omega(x, y) \tag{1.4}$$

is a constant of motion for the CR3BP. We shall refer to this constant as the energy of the system. Throughout this report, $E(L_i)$ shall denote the energy of the i^{th} Lagrange point, i.e. $E(L_i) = E(L_i^x, L_i^y, 0, 0)$. Since E is constant in the CR3BP and $(\dot{x}^2 + \dot{y}^2)$ is a nonnegative quantity, it immediatelly follows that m_3 is restricted to regions of the (x, y) plane where

$$-\Omega(x, y) \leq E. \tag{1.5}$$

Moreover, a given particle in the CR3BP is constrained to a three-dimensional energy surface $\mathcal{M} = \{(x, y, \dot{x}, \dot{y}) \mid E(x, y, \dot{x}, \dot{y}) = const.\}$ defined by its initial energy.

The Elliptic Restricted Three-Body Problem (ER3BP). A natural generalization of the CR3BP is the elliptic restricted three-body problem (ER3BP), which asks for the motion of a test particle in the presence of two *elliptically* orbiting point masses. In the ER3BP, we introduce the true anomaly $f(t)$, the angle that the line segment joining the rightmost focus of m_2's elliptical orbit to m_2's position at periapsis makes with the line segment joining that focus to m_2's position at time t (see Fig. 1.3). Normalizing units so that the pair of primary masses has unit angular

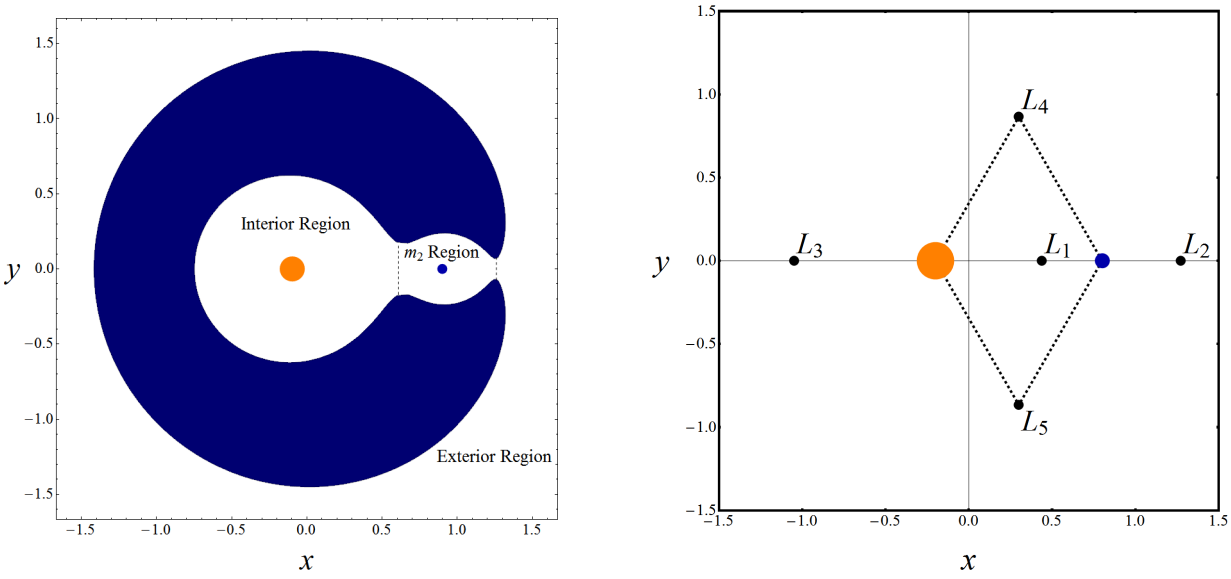

(a) (b)

Figure 1.2: (a) Regions of allowed motion (white areas) in the circular restricted three-body problem with $\mu = 0.1$, $E = -1.775$. (b) Equilibrium points L_i, $i = 1, 2, 3, 4, 5$ in the circular restricted three-body problem with $\mu = 0.1$.

momentum and the distance between the two primaries at $f = \frac{\pi}{2}$ is unity, it follows from the general solution to the two-body problem [13] that m_1 and m_2 trace out ellipses given parametrically by

$$(\bar{x}_{m_1}, \bar{y}_{m_1}) = (\frac{-\mu}{(1 + e\cos f)}\cos f, \frac{-\mu}{(1 + e\cos f)}\sin f) \tag{1.6}$$

$$(\bar{x}_{m_2}, \bar{y}_{m_2}) = (\frac{1-\mu}{(1 + e\cos f)}\cos f, \frac{1-\mu}{(1 + e\cos f)}\sin f), \tag{1.7}$$

where $(\bar{x}_{m_i}, \bar{y}_{m_i})$, $i = 1, 2$ is the position of i^{th} primary mass with respect to an inertial, barycentric coordinate frame.

It can then be shown [12] that if the true anomaly f is designated the independent variable of the system, then the equations of motion for the elliptic restricted three-body problem take the form

$$\frac{d^2x}{df^2} - 2\frac{dy}{df} = \frac{\partial\Omega}{\partial x}\Big/(1 + e\cos f) \tag{1.8}$$

$$\frac{d^2y}{df^2} + 2\frac{dx}{df} = \frac{\partial\Omega}{\partial y}\Big/(1 + e\cos f), \tag{1.9}$$

where e is the eccentricity of m_2's elliptical orbit (which is identical to that of m_1's orbit), and x and y are the coordinates of m_3 in a nonuniformly rotating, isotropically pulsating, barycentric coordinate frame in which m_1 and m_2 have fixed positions $(-\mu, 0)$ and $(1 - \mu, 0)$, respectively. We shall treat the variable f as the "time" in the ER3BP, but, to avoid ambiguity, shall use primes to denote differentiation with respect to f and dots to denote differentiation with respect to t. Note

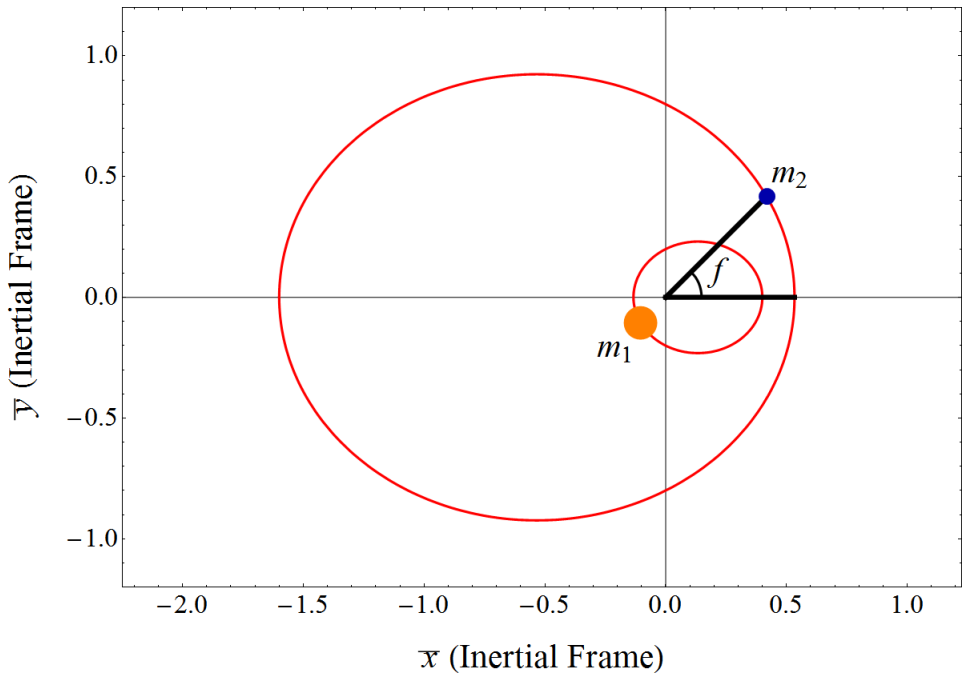

Figure 1.3: Elliptical orbits of the primary masses m_1 and m_2 in the ER3BP with respect to an inertial barycentric frame for the case $e = 0.5$, $\mu = 0.2$.

that when $e = 0$, our choice of units give $f = t$ so that equations (1.8-1.9) reduce to the equations of motion (1.1-1.2) of the circular restricted three-body problem. Thus, the CR3BP is the special case of the ER3BP in which the two primary masses have zero orbital eccentricity.

1.2 Invariant Manifolds

The presence of forbidden regions in the CR3BP permits the definition of three subsets of the (x, y) plane when $E(L_2) < E < E(L_3)$: the interior, m_2, and exterior regions, bounded approximately by the lines $x = L_1^x$, $x = L_2^x$, and the boundary of the forbidden regions (see Fig. 1.2(a)). A natural question to pose now is the following: What regulates the transport of particles between the interior, m_2, and exterior regions in the CR3BP?

Koon and co-authors [4] provide the answer to this question through analysis of the invariant manifolds of periodic orbits in the CR3BP. By linearizing the equations of motion at the collinear Lagrange points, the authors show that these equilibrium points have the stability type *saddle* $\times$ *center*. Consequently, there exists a family of periodic orbits (called Lyapunov orbits) about L_i for each $i \in \{1, 2, 3\}$, whose stable and unstable manifolds form cylindrical tubes ($S^1 \times \mathbb{R}$). Moreover, within a surface of constant energy, these tubes (as shown in Fig. 1.4) form codimension-1 separatrices between orbits with different fates: transit orbits, which exit one region and enter an adjacent region; and non-transit orbits, which remain entrapped in the region in which they began. More precisely, a particle with energy E that is currently in a given region R_A will enter an adjacent region R_B under the forward (respectively, backward) time flow if and only if that particle is inside the stable (respectively, unstable) manifold tube emanating from the unique periodic orbit

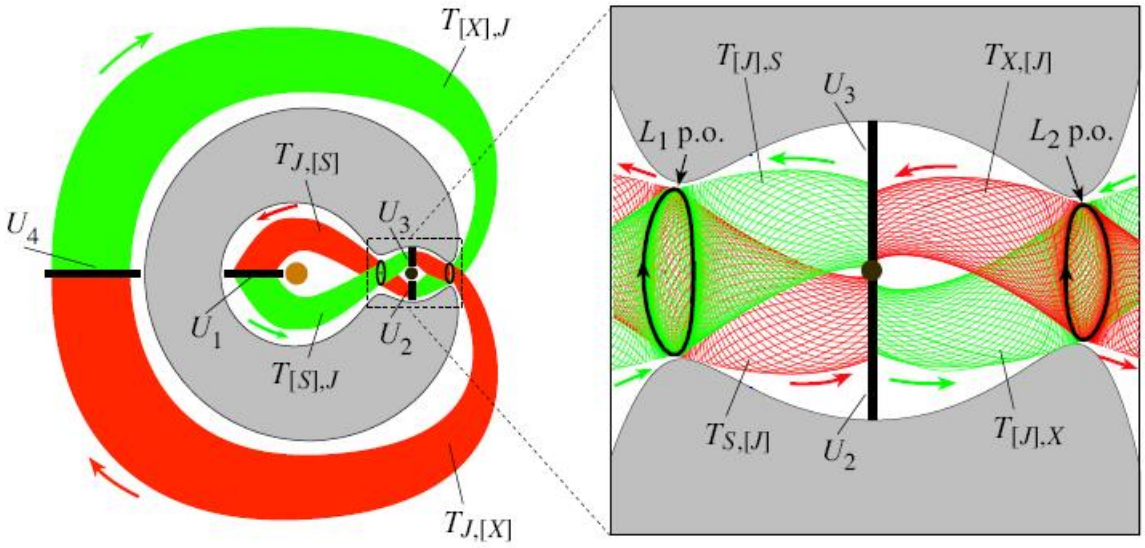

Figure 1.4: Projection of the stable (green) and unstable (red) manifold tubes in the CR3BP onto position space. Image borrowed from Koon *et al.* [4]

of energy E associated with the Lagrange point that lies on the shared boundary of regions R_A and R_B.

Computational methods for determining the CR3BP invariant manifolds are well-developed [10, 14]. To sumarize the procedure, one first constructs a periodic orbit with a specified energy using differential correction. The evolution of the periodic orbit's state transition matrix is computed over one period, and local approximations of the stable and unstable manifolds of the periodic orbit are obtained from the eigenvectors of that state transition matrix. A set of tracers in the directions of the stable and unstable eigenspaces can then be advected under the full nonlinear equations of motion to generate the invariant manifolds. The process can be curtailed by exploiting a symmetry in the CR3BP equations of motion: the mapping $(x, y, \dot{x}, \dot{y}, t) \mapsto (x, -y, -\dot{x}, \dot{y}, -t)$ is a symmetry of equations (1.1-1.2); as a result, the unstable manifold of a given Lyapunov orbit can be found by negating the y and $\dot{x}$ coordinates of every point on the corresponding stable manifold.

1.3 Lagrangian Coherent Structures (LCS)

The invariant manifolds of the CR3BP are associated with families of periodic solutions to the time-independent equations of motion (1.1-1.2). In a non-autonomous dynamical system like the ER3BP, the time-dependence of the flow precludes a direct application of the definition of an invariant manifold to the system and its limit sets. Fortunately, in many non-autonomous dynamical systems, Lagrangian coherent structures may be viewed as the time-dependent generalizations of static invariant manifolds [11].

For a continuous dynamical system with flow Φ, Lagrangian coherent structures are defined with respect to the system's finite-time Lyapunov exponent (FTLE) field, a scalar field which assigns to each point $\mathbf{x}$ in the domain a measure $\sigma(\mathbf{x})$ of the rate of divergence of trajectories with neighboring

initial conditions about that point:

$$\sigma_{t_0}^{T}(\mathbf{x}) = \frac{1}{|T|} \log \left\| \frac{d\Phi_{t_0}^{t_0+T}(\mathbf{x})}{d\mathbf{x}} \right\| \tag{1.10}$$

Separatrices can be associated with high FTLE values, since neighboring trajectories on opposite sides of a separatrix tend to diverge most quickly. Hence, Lagrangian coherent structures are defined as ridges (curves—or, more generally, codimension-1 surfaces in systems with arbitrary dimension—in the domain whose images in the graph of the FTLE field satisfy certain conditions that formalize intuitive notions of a ridge; see Lekien *et al.* [15] for details) in the system's FTLE field. These time-varying ridges form barriers between the almost invariant sets of the domain and can be viewed as the non-autonomous analogues of time-independent invariant manifolds.

In practice, the derivative of the flow with respect to initial position is computed via finite differencing for a grid of initial positions $\mathbf{x}$, whose trajectories over the interval $[t_0, t_0 + T]$ are calculated numerically.

Note that (1.10) permits the computation of a backward-time FTLE through the use of a negative integration length T. A ridge in such a backward-time FTLE field (which we distinguish from forward-time FTLE ridges with the names *attracting LCS* for the former, *repelling LCS* for the latter) corresponds to the time-dependent analogue of an unstable manifold. A symmetry in the ER3BP equations of motion, akin to the CR3BP symmetry described previously, eliminates the need to compute backward-time FTLE fields: noting that the cosine function is an even function, it is easy to check that the mapping $(x, y, x', y', f) \mapsto (x, -y, -x', y', -f)$ is a symmetry of equations (1.8-1.9); as a result, any attracting LCS in the ER3BP can be found by negating the y and x' coordinates of every point on the corresponding repelling LCS and viewing its evolution in reverse time. Moreover, equations (1.8-1.9) are periodic with period 2π. Thus, the Lagrangian coherent structures in the ER3BP need only be computed over the interval $0 \leq f < 2\pi$; an LCS at any other epoch $\tilde{f}$ can be identified with the LCS at the time $f \in [0, 2\pi)$ congruent to $\tilde{f}$ modulo 2π.

On that note, it is worth mentioning that the periodicity of the ER3BP equations of motion (1.8-1.9) means that one could, in principle, obtain the results presented in this report using standard manifold globalization techniques. Indeed, consider the map $\Phi_{f_0}^{f_0+2\pi}$, where Φ denotes the flow of equations (1.8-1.9) and $f_0 \in [0, 2\pi)$ is a fixed true anomaly. This map defines a defines a discrete dynamical system on the Poincaré section $U_{f_0} = \{(x, y, x', y', f) \mid f = f_0\}$ of the ER3BP's augmented phase space. Using the methods of [10], one could extract invariant manifolds from U_{f_0} for a series of initial epochs f_0 and conceivably replicate the LCS animations presented in this report. The reader should bear in mind, however, that there are more general situations (e.g., the four-body problem in the case where the ratio of the periods of the two smaller primary masses is irrational) in which LCS analysis applies even though the aperiodicity of the flow eliminates the possibility of using the method just described.

2 Computational Methodology

A key obstacle encumbering the investigation of Lagrangian coherent structures (LCS) in the elliptic restricted three-body problem (ER3BP) is the dimension of the system under examination. In contrast to the CR3BP, where the existence of a constant of motion restricts the motion of the test particle to a three-dimensional energy surface within which there exist cylindrical invariant

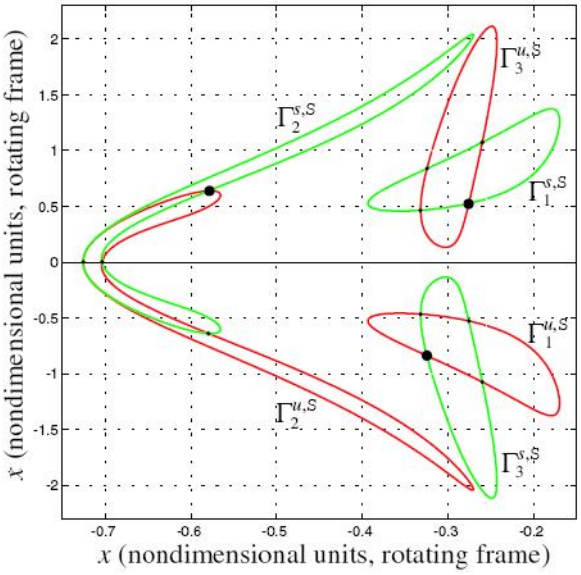

Figure 2.1: Intersection of the stable (green) and unstable (red) manifold tubes in the CR3BP with the plane $y = 0$ (within a surface of constant energy). Here $\mu = 0.1$ and $E = E(L_1) + .03715$. Subscripts denote the order of intersection of the manifolds with the plane. Image borrowed from Koon *et al.* [4]

manifolds, the ER3BP possesses no integrals of motion. Thus, any LCS in the ER3BP is formally a three-dimensional surface contained in the ER3BP's four-dimensional phase space. As an extraction and visualization of such a structure would be difficult, we explore two means of circumventing this obstacle.

2.1 Poincaré Maps and the Finite-Iteration Lyapunov Exponent

One such method utilizes Poincaré sections to reduce the dimension of the system by one. Selecting a three-dimensional hyperplane $U \subset \mathbb{R}^4$ and seeding a subset $U_0 \subset U$ with a grid of tracers, we can advect these tracers under the flow until the their orbits' (directed) N^{th} intersections with the hyperplane are reached. It then becomes feasible to compute a finite-iteration Lyapunov exponent (FILE)

$$\sigma^N(\mathbf{x}) = \frac{1}{|N|} \log \left\| \frac{d\mathbf{P}^N(\mathbf{x})}{d\mathbf{x}} \right\| \tag{2.1}$$

for each point $\mathbf{x} \in U_0$, where the function $\mathbf{P} : U \to U$ is the one-sided Poincaré map associated with the plane U and the flow Φ of equations (1.8-1.9). We shall refer to this method as the Poincaré map method, its associated field being an FILE field.

2.2 The Finite-Time Lyapunov Exponent

Alternatively, it is possible to compute four-dimensional FTLE fields and examine three-dimensional cross-sections of these fields. We shall refer to this method as the cross-sectional method, its associated field being an FTLE field.

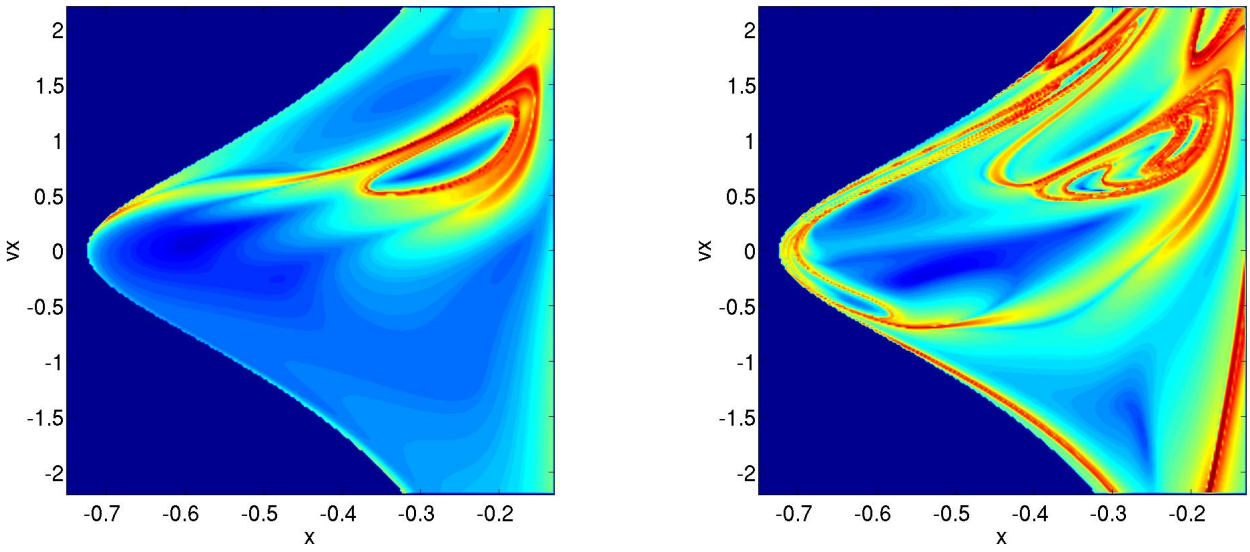

(a) (b)

Figure 2.2: FTLE field contour plot (i.e., generated using a cross-sectional FTLE calculation) in the CR3BP (within a surface of constant energy) at the plane $y = 0$ with integration time (a) $T = 2$ and (b) $T = 5$. Energy and mass parameters are identical to those in Fig. 2.1. Observe that increasing integration time reveals the second intersection $\Gamma_2^{s,\mathrm{S}}$ of the stable manifold of the L_1 Lyapunov orbit, as well as some additional curves of high FTLE.

2.3 A Comparison Using the Circular Restricted Three-Body Problem (CR3BP) as a Test Bed

In order to gauge the performance of these two methods, we first apply them to a simpler, lower dimensional system, namely the CR3BP equations of motion with a fixed energy E. Since the invariant manifolds of the CR3BP are examined in considerable detail in Koon *et al.* [4], it helps to compare the outputs of the two methods with published data. Fig. 2.1, taken from Koon *et al.* [4], shows the intersection of the stable and unstable manifold tubes of the Lyapunov orbit about L_1 for a fixed energy just above $E(L_1)$. Throughout this report, we adopt the notation of Koon and co-authors [4]: $W^s_{L_1,\mathrm{p.o.}}$ and $W^u_{L_1,\mathrm{p.o.}}$ denote the stable and unstable manifolds, respectively, of the L_1 Lyapunov orbit, and $\Gamma_i^{s,\mathrm{S}}$ and $\Gamma_i^{u,\mathrm{S}}$ denote the i^{th} intersection of $W^s_{L_1,\mathrm{p.o.}}$ and $W^u_{L_1,\mathrm{p.o.}}$, respectively, with the plane $y = 0$ in the interior region within a surface of constant energy. (The capital S in $\Gamma_i^{s,\mathrm{S}}$ specifies that this intersection lies in the interior, or "Sun," region.)

Fig. 2.2(a) plots the CR3BP FTLE field along the plane $y = 0$ (within a surface of constant energy) for an integration time $T = 2$, as computed using the cross-sectional method. As expected, large FTLE values can be observed at the first intersection $\Gamma_1^{s,\mathrm{S}}$ of the stable manifold $W^s_{L_1,\mathrm{p.o.}}$ of the L_1 Lyapunov orbit. Increasing the integration time T (Fig. 2.2(b)) unveils the subsequent intersection $\Gamma_2^{s,\mathrm{S}}$ of the same stable manifold.

For comparison, the FILE field for the first three iterations of the Poincaré map associated with the plane $y = 0$ (within a surface of constant energy) are shown in Fig. 2.3. In analogy with

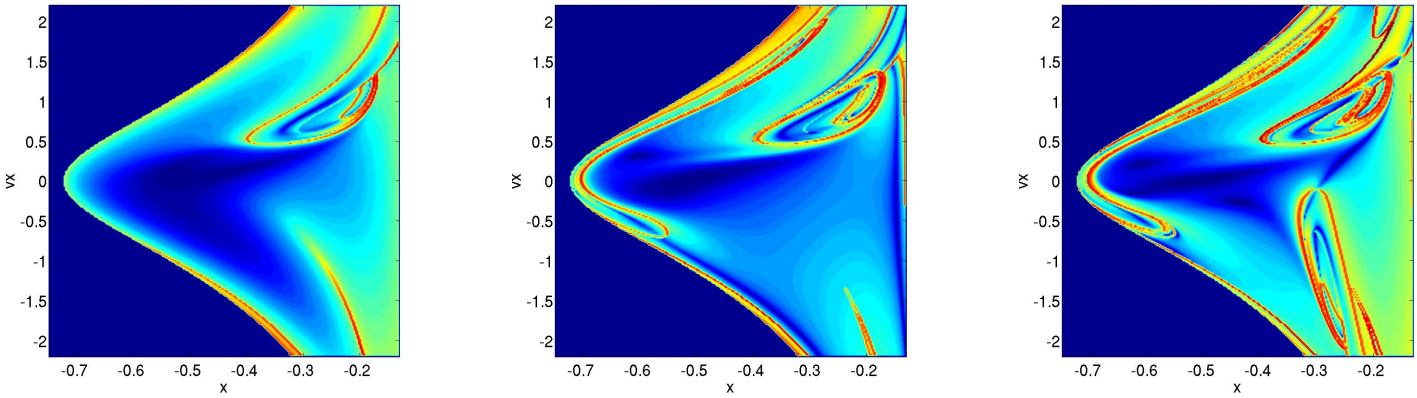

(a) (b) (c)

Figure 2.3: FILE field contour plot (i.e., generated using a Poincaré map calculation) in the CR3BP (within a surface of constant energy) at the plane $y = 0$ for iterations (a) $N = 1$, (b) $N = 2$, and (c) $N = 3$. Again, energy and mass parameters are identical to those in Fig. 2.1. Notice the superfluous FILE ridges caused by a lack of transversality between orbits and the surface of section in, for instance, the lower right-hand corners of (a) and (b). Unsurprisingly, larger iteration numbers N reveal the higher order intersections $\Gamma_2^{s,\mathrm{S}}$ and $\Gamma_3^{s,\mathrm{S}}$ of the stable manifold of the L_1 Lyapunov orbit.

increasing integration time, increasing the iteration number N successively unveils the higher order intersections $\Gamma_1^{s,\mathrm{S}}$, $\Gamma_2^{s,\mathrm{S}}$, and $\Gamma_3^{s,\mathrm{S}}$ of $W^s_{L_1,\mathrm{p.o.}}$ with the plane $y = 0$.

Notice that the FILE field has a significant drawback: in addition to locating transport barriers associated with stable manifolds of limit sets, the FILE field also exhibits ridges where the Poincaré map is not differentiable due to a lack of transversality between orbits and the plane of interest. Indeed, for initial points on the Poincaré section whose orbits do not intersect the surface of section transversally upon their return, differentiabilty is not guaranteed and the FILE loses its meaning. Unfortunately, for a given FILE field, these structures appear indistinguishably from genuine transport barriers and bear little or no influence on the dynamics of the system. Furthermore, the Poincaré map $\mathbf{P}$ is in general only defined for a subset of the surface of section U. For these reasons, we have adopted the cross-sectional method as the standard for all subsequent computations.

3 Lagrangian Coherent Structures (LCS) in the Elliptic Restricted Three-Body Problem (ER3BP)

The computational tools developed in the previous section make possible the presentation of the main results of this study, Lagrangian coherent structures (LCS) in the elliptic restricted three-body problem (ER3BP). Recall that in the ER3BP, whose equations of motion are non-autonomous and possess no integrals of motion, the notions of constant-energy surfaces lose their relevance, and hence we must examine the time-dependent analogues of $W^s_{L_1,\mathrm{p.o.}}$ and $W^u_{L_1,\mathrm{p.o.}}$ in the full four-dimensional phase space, where the plane $y = 0$ is three-dimensional. An important question to ask at this moment is the following: What will the intersection of $W^s_{L_1,\mathrm{p.o.}}$ with plane $y = 0$ in the

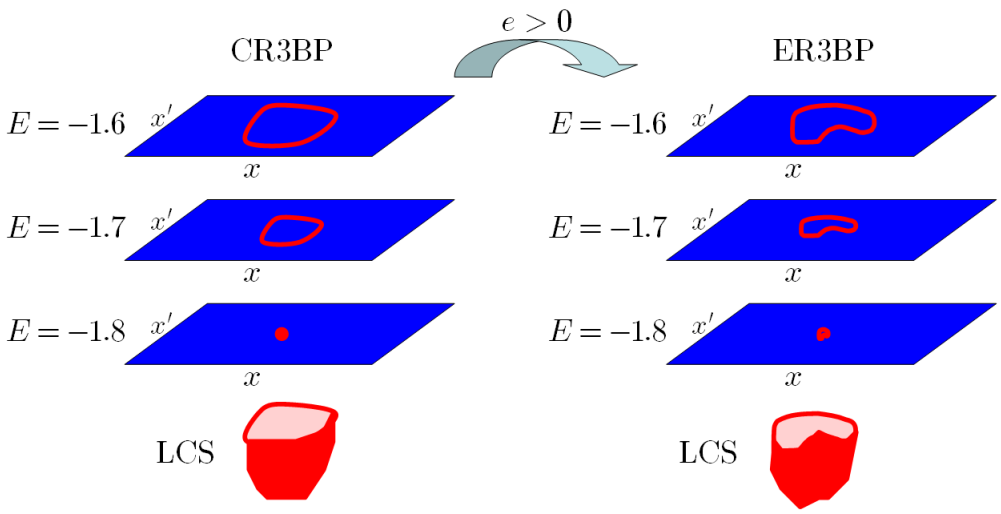

Figure 3.1: Illustration of the hypothesis that, in terms of the coordinates x, y, x', and E, the intersection of the plane $y = 0$ with the LCS corresponding to the analogue of $W^s_{L_1,\text{p.o.}}$ might appear as a distorted paraboloid in the ER3BP.

interior region look like? The answer to this question depends crucially on our choice of coordinate system.

Let

$$E(x, y, x', y') = \frac{1}{2}(x'^2 + y'^2) - \frac{\Omega}{1 + e\cos f}, \tag{3.1}$$

where, in the notation mentioned previously, x' and y' have been used to denote the quantities $\frac{dx}{df}$ and $\frac{dy}{df}$, respectively. Notice that when $e = 0$, (3.1) reduces to the expression for the energy in the CR3BP given in equation (1.4). We shall refer to this quantity as the "energy" in the ER3BP, with the hopes that this notation will give the reader a better sense of the correlation between the quantities defined here and their CR3BP analogues. In actuality, (3.1) is the ER3BP's Hamiltonian.

Choosing a coordinate system (x, y, x', E) to parametrize phase space in the ER3BP (so that the plane $y = 0$ is parametrized by x, x', and E) allows for a natural means of extending the qualitative results of LCS studies in the CR3BP. For fixed values of E at the plane $y = 0$, $x < 0$, a ridge in the FTLE field on the $(x, x', y = 0, E = const.)$ plane should appear as a closed curve, corresponding to a perturbed version of $\Gamma_1^{s,\text{S}}$ (the perturbation arising from the fact that the eccentricity e is nonzero). Since the amplitude of an L_1 Lyapunov orbit in the CR3BP is roughly proportional to the square root of its energy minus $E(L_1)$, we should expect that this closed curve will shrink with decreasing E and that for some critical energy the curve will contract to a point. Consequently, the intersection of the LCS with the plane $y = 0$ might appear as a distorted paraboloid, provided we parametrize phase space with the coordinates x, y, x', and E. See Fig. 3.1 for an illustration of this notion.

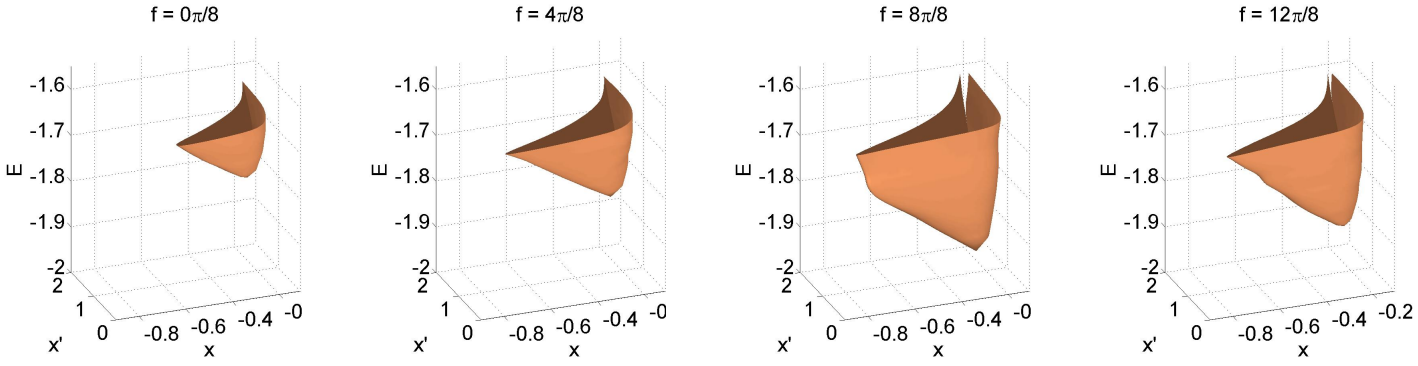

Figure 3.2: Intersection of the plane $y = 0$ with the LCS corresponding to the time-dependent analogue of $W^s_{L_1,\text{p.o.}}$ in the ER3BP with mass ratio $\mu = 0.1$, orbital eccentricity $e = 0.04$. See LCS-ER3BP.mov to view the full sequence of images in animated format.

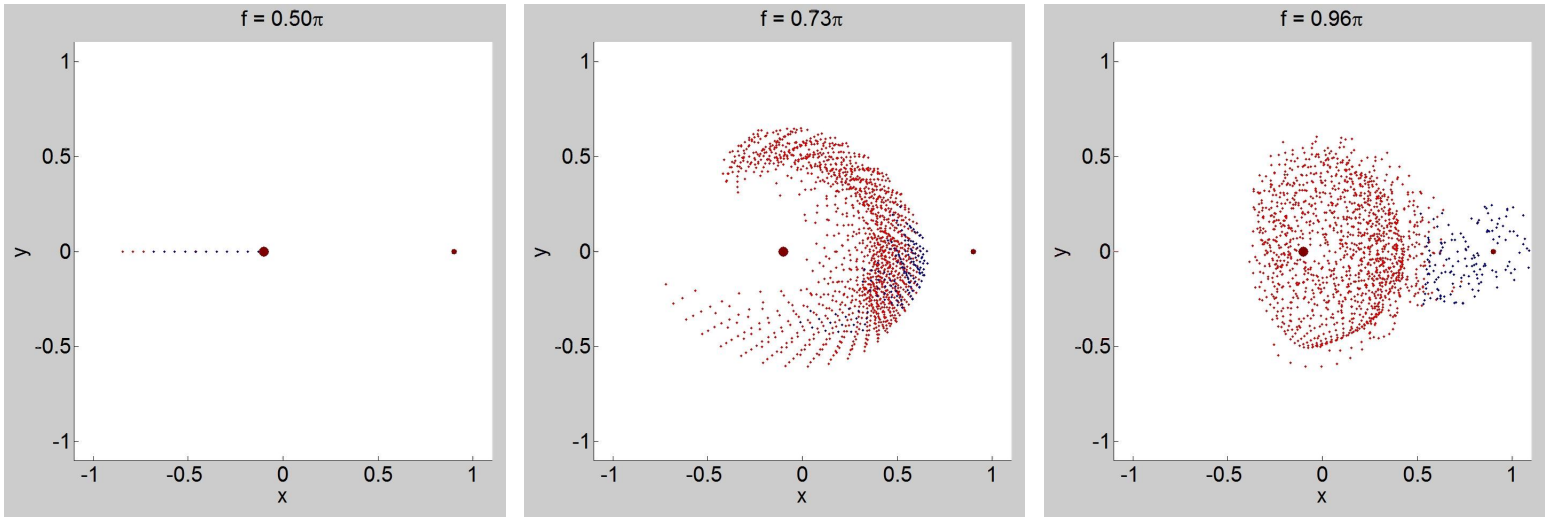

Figure 3.3: Snapshots of the motion of a collection of tracers colored based upon their initial location relative to the LCS in Fig. 3.2. The tracers were seeded at true anomaly $f = \pi/2$ over a $15 \times 15 \times 15$ (x, x', E) grid on the plane $y = 0$ and advected forward in time. Blue tracers began inside the LCS "bowl," while red tracers began outside the LCS "bowl." See Tracers.avi to view the full sequence of images in animated format.

3.1 A Test Case

Fig. 3.2 displays snapshots of the intersection of the plane $y = 0$ with the LCS corresponding to the analogue of $W^s_{L_1,\text{p.o.}}$ under a set of fabricated parameters (mass ratio $\mu = 0.1$, orbital eccentricity $e = 0.04$). The video LCS-ER3BP.mov shows the full sequence of images in animated format. The LCS was extracted from an FTLE field generated by advecting tracers over an integration length $T = 2.5$, roughly $\frac{2}{5}$ of the orbital period of the two primary masses. As expected, the LCS forms a distorted paraboloid that pulsates with time. The key property of this LCS is that, like $W^s_{L_1,\text{p.o.}}$ of the CR3BP, this LCS separates orbits that enter m_2's "sphere of influence" from orbits that do not.

To help visualize the role that this LCS plays in the dynamics of the ER3BP, Fig. 3.3 displays

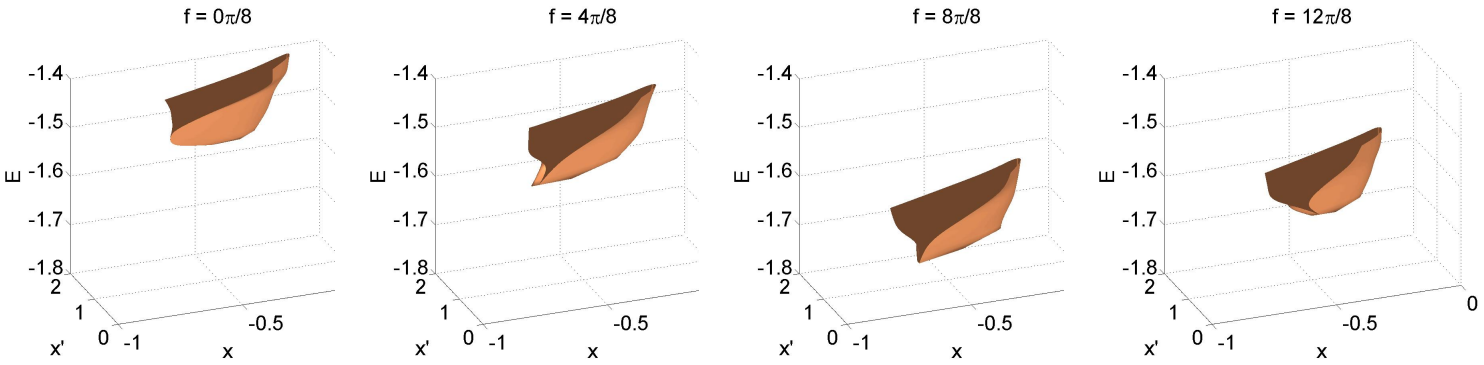

Figure 3.4: Intersection of the plane $y = 0$ with the LCS corresponding to the time-dependent analogue of $W^s_{L_1,\text{p.o.}}$ in the Earth-Moon-spacecraft system (mass ratio $\mu \approx 0.012$, orbital eccentricity $e \approx 0.055$). See LCS-ER3BP-Earth-Moon.mov to view the full sequence of images in animated format.

snapshots of the motion of a collection of tracers that have been colored based upon their initial location relative to the LCS. The tracers were seeded at true anomaly $f = \pi/2$ over a $15 \times 15 \times 15$ (x, x', E) grid on the plane $y = 0$ and advected forward in time. Blue tracers began inside the LCS "bowl," while red tracers began outside the LCS "bowl." The video Tracers.avi shows the full sequence of images in animated format.

3.2 LCS in the Earth-Moon System

The Earth-Moon-spacecraft system (mass ratio $\mu \approx 0.012$, orbital eccentricity $e \approx 0.055$) provides an excellent physical system for which ER3BP LCSs can be examined. In this case (see Fig. 3.4 and the video LCS-ER3BP-Earth-Moon.mov), the intersection of the plane $y = 0$ with the LCS corresponding to the analogue of $W^s_{L_1,\text{p.o.}}$ is smaller than in the case above, which is to be expected given the lower mass ratio μ in the Earth-Moon system. It is also evident that this LCS is not as clean as in the case above, perhaps owing to integration error or to a genuine decay in the precision of the boundary separating transit orbits from non-transit orbits.

3.3 Mercury and the BepiColombo Mission

The planet Mercury embodies the necessity of the use of the elliptic restricted three-body approximation over the circular restricted three-body approximation in the simulation of certain celestial systems. With a value slightly larger than 0.2, Mercury's orbital eccentricity is more than twice that of any other planet in the solar system (excluding Pluto) [16]. It follows that the design of a Mercury-bound space mission relies heavily on ER3BP dynamics. Indeed, the European Space Agency's (ESA) BepiColombo mission, a mission to Mercury scheduled to launch in 2013, intends to utilize solar perturbations to achieve Mercurial capture of the spacecraft [17]. Naturally, one might expect such a trajectory to share an intimate connection with Lagrangian coherent structures in the Sun-Mercury-spacecraft ER3BP. As the following discussion reveals, this intuition is correct.

Fig. 3.5 displays the FTLE field at a cross section of phase space in the spatial elliptic restricted three-body problem (with Sun-Mercury-spacecraft parameters), juxtaposed with the intersection of ESA's BepiColombo trajectory[1] with that cross section. Specifically, the cross section shown is the

[1]Baseline trajectory for launch in 2012 [18].

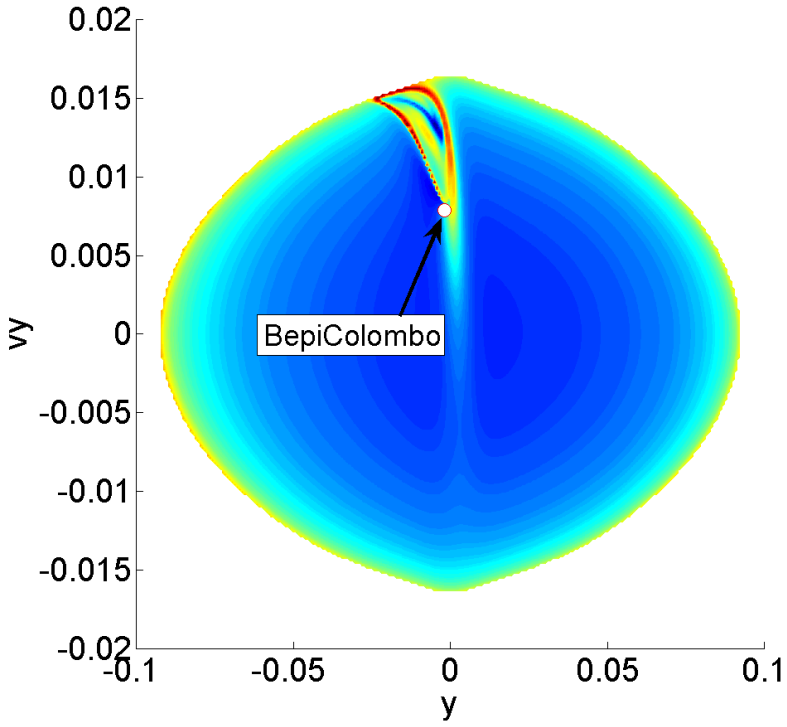

Figure 3.5: Snapshot of the FTLE field at a cross section of phase space in the spatial elliptic restricted three-body problem (with Sun-Mercury-spacecraft parameters), juxtaposed with the intersection of BepiColombo's trajectory with that cross section.

plane $x = 0.99$, $z = 0.0007$, $z' = -0.0003$, $E = -1.7613$ at epoch $f = 3.9065$ in normalized units, which is to the left of the Sun-Mercury L_1 (See Fig. 3.6 for an illustration). Note that we have worked with the spatial ER3BP [12] rather than the planar ER3BP for this computation to account for the nonplanarity of BepiColombo's orbit. The LCS seen in Fig. 3.6 is the time-dependent analogue of the stable manifold of the L_1 Lyapunov orbit in the circular restricted three-body problem. Notice the remarkable manner in which BepiColombo's trajectory straddles the LCS. This should come as no surprise, given that this particular LCS governs transport between the interior (Sun) region and the m_2 (Mercury) region. Clearly, Lagrangian coherent structures in the three-body problem can serve as valuable guides for mission design; they often enclose regions of phase space whose composite trajectories exhibit a desirable characteristic—in this instance, eventual entrance into the m_2 (Mercury) region. This notion paves the way for the use of LCS computation in conjunction with optimal control algorithms for space mission design. Using Lagrangian coherent structures to guide the selection of initial guesses for trajectory optimization problems should offer a powerful means of exploiting the fuel-efficient pathways of the Interplanetary Transport Network.

Finally, we note that the notion that BepiColombo's trajectory straddles an LCS of the spatial elliptic restricted three-body problem correlates well with previous studies of the BepiColombo mission. Campagnola & Lo [18] have recognized that if one perturbs certain ER3BP quasiperiodic orbits about the Sun-Mercury L_1 in the direction of minimal stretching and examines the perturbed orbits' trajectories under the backward time flow (in a manner analogous to the traditional method

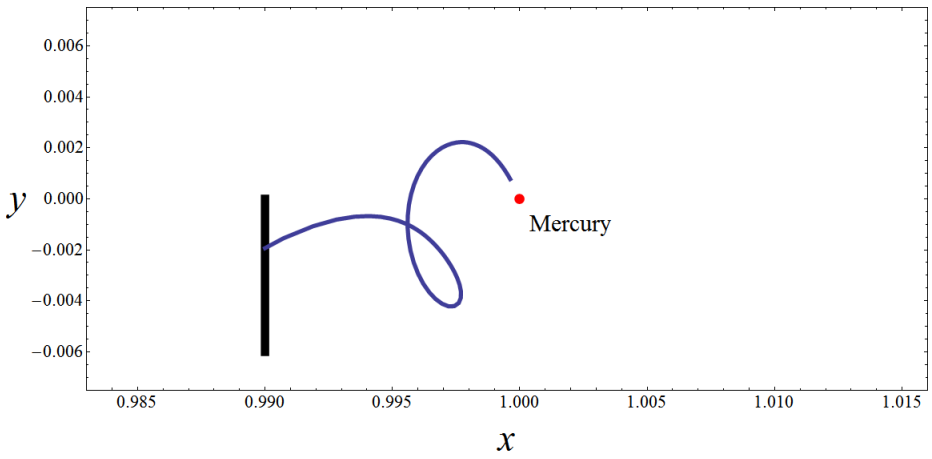

Figure 3.6: A portion of BepiColombo's trajectory (projected onto the x-y plane). The vertical black line segment represents the location of the cross section used in Fig. 3.5.

of globalizing stable manifolds in the CR3BP), the resulting trajectories closely shadow the route of BepiColombo. This is best understood by noting the relationship between LCS of time-dependent systems and invariant manifolds of their associated time-independent augmentations: For a non-autonomous system $\dot{\mathbf{q}} = \mathbf{f}(\mathbf{q}, t)$, we can identify Lagrangian coherent structures at any given instant as the constant-time cross-sections of static invariant manifolds of the associated augmented system $\dot{\tilde{\mathbf{q}}} = \tilde{\mathbf{f}}(\tilde{\mathbf{q}})$, where $\tilde{\mathbf{q}} = (\mathbf{q}, t)$ and $\tilde{\mathbf{f}}(\tilde{\mathbf{q}}) = (\mathbf{f}(\mathbf{q}, t), 1)$. Consequently, we can expect tracers lying on repelling LCSs to approach invariant structures of the augmented system under the forward time flow. In our case, the limit sets of the augmented system correspond precisely to the quasiperiodic orbits, periodic orbits, and fixed points of the ER3BP.

4 Conclusions and Further Study

The results presented in this report demonstrate the existence of periodically pulsating Lagrangian coherent structures in the phase space of the elliptic restricted three-body problem which arise as the time-dependent analogues of stable and unstable manifolds of periodic orbits in the circular restricted three-body problem. The examination of cross-sections of full-dimensional finite-time Lyapunov exponent fields proves to be an effective method of computing the intersections of these structures with surfaces of section in the ER3BP phase space, whose high dimension precludes the visualization of entire LCSs. As a concrete application, these results reveal the influence of orbital eccentricity on segments of the Interplanetary Transport Network associated with elliptically orbiting mass pairs.

Interestingly, LCS pulsation in the cases presented is characterized almost entirely by sinusoidal translation in E. An analytical explanation of this observation seems a worthy topic for further study. In addition, an investigation of the dual role that these structures play as both separatrices and as the invariant manifolds of quasiperiodic orbits deserves consideration; an interesting, albeit unsurprising, phenomenon is the observation that any tracer that lies on an ER3BP LCS eventually tends toward a quasiperiodic orbit.

From a computational perspective, ridge extraction from three-dimensional FTLE fields presents

a formidable challenge in a study such as this. The design of an automated ridge extraction algorithm for arbitrary-dimensional scalar fields would constitute an important advancement for the LCS community.

The use of a symplectic integrator might benefit this study, as the ER3BP is a Hamiltonian system. It is well-known that in the context of the numerical simulation of mechanical systems, structure-preserving integration algorithms such as variational integrators exhibit several desirable properties that traditional integration schemes generally do not, including exact momentum conservation, accurate energy behavior, and symplecticity [19]. The extent to which such properties may influence the results of LCS computations for mechanical systems like the three-body problem is an issue yet to be studied in detail.

Finally, and perhaps most importantly, the computation of Lagrangian coherent structures in conjunction with the use of optimal control algorithms constitutes a potentially powerful tool for space mission design. LCS computation provides a general method for computing separatices in celestial systems that may or may not exhibit time dependence, offering a broader, less restrictive technique than the traditional manifold globalization approach that relies on the precalculation of limit sets. In turn, these separatrices serve to guide the selection of initial guesses for trajectory optimization problems. The results reported in Section 3.3 illustrate this assertion, demonstrating the close relationship between LCS in the three-body problem and the Mercurial approach portion of ESA's BepiColombo mission. In almost any mission of this type, multi-body dynamics play an integral role. It should be clear that the low-energy pathways which arise naturally in the study of the three-body problem are not merely mathematical curiosities; they offer a practical and tractable means of overcoming the intrinsic challenges of space mission design.

References

[1] Dellnitz, M. *et al.* Transport in dynamical astronomy and multibody problems. *International Journal of Bifurcation and Chaos* **15**, 699-727 (2005).

[2] Porter, M. A. & Cvitanović P. Ground control to Niels Bohr: exploring outer space with atomic physics. *Notices of the American Mathematical Society* **52**, 1020-1025 (2005).

[3] Haller, G. Distinguished material surfaces and coherent structures in three-dimensional fluid flows. *Physica D* **149**, 248-277 (2001).

[4] Koon, W. S., Lo, M., Marsden, J. E. & Ross, S. D. Heteroclinic connections between periodic orbits and resonance transitions in celestial mechanics. *Chaos* **10**, 427-469 (2000).

[5] Marsden, J. E. & Ross, S. D. New methods in celestial mechanics and mission design. *Bulletin of the American Mathematical Society* **43**, 43-73 (2005).

[6] Koon, W. S., Lo, M. W., Marsden, J. E. & Ross, S. D. Resonance and capture of Jupiter comets. *Celestial Mechanics and Dynamical Astronomy* **81**, 27-38 (2001).

[7] Gómez, G., Koon, W. S., Lo, M. W., Marsden, J. E., Masdemont, J. & Ross, S. D. Connecting orbits and invariant manifolds in the spatial restricted three-body problem. *Nonlinearity* **17**, 1571-1606 (2004).

[8] Koon, W. S., Lo, M. W., Marsden, J. E. & Ross, S. D. Dynamical systems, the three-body problem, and space mission design. *International Conference on Differential Equations*, Berlin, 1999, (Fiedler, B., Grger, K. & Sprekels, J. eds.), World Scientific, 1167-1181 (2000).

[9] Koon, W. S., Lo, M. W., Marsden, J. E. & Ross, S. D. The Genesis trajectory and heteroclinic connections. *AAS/AIAA Astrodynamics Specialist Conference*, Girdwood, Alaska, 1999, AAS 99-451 (1999).

[10] Parker, T. S. & Chua L. O. *Practical Numerical Algorithms for Chaotic Systems*, (Springer-Verlag, New York, 1989).

[11] Shadden, S. C., Lekien, F. & Marsden, J. E. Definition and properties of Lagrangian coherent structures from finite-time Lyapunov exponents in two-dimensional aperiodic flows. *Physica D* **212**, 271-304 (2005).

[12] Szebehely, V. G. *Theory of Orbits: The Restricted Problem of Three Bodies*, (Academic Press, New York, 1967).

[13] Goldstein, H., Poole, C. & Safko, J. *Classical Mechanics* (Addison Wesley, San Fransisco, 2002).

[14] Ross, S. D. "Cylindrical Manifolds and Tube Dynamics in the Restricted Three-Body Problem" (PhD thesis, California Institute of Technology, 2004).

[15] Lekien, F., Shadden S. C., & Marsden, J. E. Lagrangian coherent structures in n-dimensional systems. *Journal of Mathematical Physics* **48**, 1-19 (2007).

[16] Yeomans, D. K. Solar System Dynamics. *NASA Jet Propulsion Laboratory* http://ssd.jpl.nasa.gov/

[17] Jehn, R., Campagnola, S., Garcia, D. & Kemble, S. Low-thrust approach and gravitational capture at Mercury. *18th International Symposium on Space Flights Dynamics*, Munich, Germany, 1-6 (2004).

[18] Campagnola, S. & Lo, M. BepiColombo gravitational capture and the elliptic restricted three-body problem. *18th ICIAM07 6th International Congress on Industrial and Applied Mathematics*, Zurich, Switzerland, 2007, 1-2 (2007).

[19] Marsden, J. E. & West, M. Discrete mechanics and variational integrators. *Acta Numerica* **10**, 357-514 (2001).